

Wetting phase diagrams of a polyacid brush with a triple pointA. A. Mercurieva,¹ P. Iakovlev,^{1,2} E. B. Zhulina,¹ T. M. Birshtein,¹ and F. A. M. Leermakers²¹*Institute of Macromolecular Compounds, St. Petersburg 1990004, Russia*²*Laboratory of Physical Chemistry and Colloid Science, Wageningen University, Dreijenplein 6, 6703 HB Wageningen, The Netherlands*

(Received 21 June 2006; published 15 September 2006)

The (pre)wetting behavior of an annealed polyelectrolyte (PE) brush by an electrolyte solution that is strongly segregated from an apolar phase is analyzed. In this complex interface, there are interactions on various length scales. There are short-range interactions with the (uncharged) surface, and there are interactions on the length scale of the brush height. Using either the ionic strength or the water-surface interaction strength as the control parameters, it is possible to approach and induce a wetting transition in this system. The first-order wetting transition, promoted by favorable short-range substrate interactions with the surface, is in competition with the wetting transition controlled by the detachment of the fluid interface from the periphery of the PE brush. The electric double layer on top of the PE brush contributes with a repulsive forces to the disjoining pressure that tends to thicken the wetting film, and therefore, the transition in all cases is first order. Various phase portraits of the wetting phase diagram are envisioned. One of these features the crossing of two prewetting lines. At the crossing point three surface states coexist. This triple point is analyzed in some detail with the help of a molecular-level self-consistent field model.

DOI: [10.1103/PhysRevE.74.031803](https://doi.org/10.1103/PhysRevE.74.031803)

PACS number(s): 82.35.Rs, 68.08.Bc, 68.47.Pe, 64.60.Cn

I. INTRODUCTION

The technological importance of dense layers of end-grafted polymer chains, so-called polymer brushes, cannot be overestimated. A polymer brush is put on top of a surface with the goal of tuning it to become compatible to the medium, making it functional, preventing its fouling, reducing the friction, inducing repulsive forces between particles, or modifying the wetting characteristics of a surface. In this paper, we will discuss the wetting of an annealed polyelectrolyte (PE) brush. More specifically our attention is drawn to the wetting phase diagram, which has unusual features. From the wetting phase diagram, one can read how the free energy landscape is structured, i.e., whether or not a growing wetting film may experience significant kinetic barriers. We will show that for the PE brush this free energy landscape can be far from smooth.

In wetting studies, one challenges an interface of interest to a binary mixture of liquids that has a solubility gap. These liquids may generically be called “oil” and “water.” Typically one is interested in how a wetting film develops when the wetting compound, which is the minority compound in the system, is added to the system. The surface covered by the brush presents interactions to the wetting component on more than one length scale. First of all, the wetting component has interactions with the substrate. These occur on a short range (distances of order the size of the water molecules). Second, there are interactions with the brush (solvation). As the height of the brush is of order of the chain length, these interactions may indeed be long range. In addition, there may be a van der Waals contribution that gives a repulsive or an attractive contribution to the disjoining pressure in the film, which tends to thicken or thin the wetting (water) film in between the surface and the oil phase [1]. The van der Waals force decays as a power law and is thus relatively long range. This is a problem in fundamental wetting

studies dedicated to find ways to manipulate the wetting phase diagrams.

Recently, we argued that when the substrate is made of a polymer gel swollen by the wetting component, the van der Waals interactions are essentially absent [2,3]. The same must be true when the gel is made of cross-linked polyelectrolytes. Such polymer gels are unique systems to study wetting in the absence of van der Waals forces (or formally better: in the micro van der Waals force regime). Alternatively, one can take the height of the brush sufficiently large such that the van der Waals forces will have hardly any influence on the wetting behavior. This means that it is completely determined by the (tunable) brush. Below we will therefore assume that the van der Waals contribution can safely be ignored.

Our favorite way to investigate the wetting behavior is to study (or compute) adsorption isotherms. In an adsorption isotherm, one presents the adsorbed amount of the wetting component Γ_w (e.g., the excess amount per unit area) as a function of the concentration of the wetting compound in the solvent mixture or, equivalently, the chemical potential of the wetting compound μ_w . The adsorbed amount is an increasing function of the chemical potential. Of relevance is to know what happens when the concentration of the wetting compound reaches its saturation value at $\mu_w^\#$ (the bulk binodal value) with the adsorbed amount $\Gamma_w^\#$. If $\Gamma_w^\#$ diverges, the surface is *wet*. If $\Gamma_w^\#$ remains finite, the surface is in a nonwet state; the system is in the partial wetting regime. Transitions from the nonwet to the wet state are called wetting transitions.

The classical wetting theory [4] (which deals with interactions on just one length scale) shows that the wetting transition can be first or second order. A second-order wetting transition, e.g., generated by a change of the temperature T , is characterized by the fact that $\Gamma_w^\#$ smoothly and continuously goes from a finite to an infinite value upon the ap-

proach of the wetting transition at T^W . In a first-order wetting transition, however, the adsorbed amount at coexistence $\Gamma_W^\#$ remains finite for $T < T^W$ and jumps to infinite at $T = T^W$. In a mean-field theory, such a jump is accompanied by a van der Waals loop in the adsorption isotherm. For $T > T^W$, the van der Waals loop occurs at a chemical potential μ_W^* lower than the saturation value, i.e., for $\mu_W^* < \mu_W^\#$. Sufficiently above the wetting transition, the step in the isotherm disappears and the adsorbed amount smoothly and monotonically increases as a function of the chemical potential. The collection of all $\mu_W^*(T)$ points presents a line in a wetting phase diagram. This line is called the prewetting line. It starts at T^W , where $\mu_W^* = \mu_W^\#$, and ends in the critical endpoint. In this paper, we are interested in the prewetting features of the PE brush. Our control parameters are the ionic strength and the water-surface interaction strength.

In a series of papers, we proved that the wetting of a neutral polymer brush onto a substrate by a wetting component that strongly segregates from a majority liquid has various intricacies [2,5,6,8]. As the binary mixture of solvents is taken far from the critical point, the wetting transition with a solid substrate (i.e., in the absence of the brush) is strongly first-order. This means that one should expect a prewetting line in the phase diagram due to this. However, the brush presents also interactions on a larger length scale and the interactions on the longest length scale eventually determine whether the surface is wet or not. We have shown before that the wetting transition of the brush is strongly coupled to the adsorption of the polymer brush chains onto the water-oil interface [2]. If the chains adsorb onto this interface, we should expect chains grafted with one end to the substrate bridging to the thin wetting film and reach the water-oil interface. This bridging effect causes an attractive contribution to the disjoining pressure, and thus, there is partial wetting. When, by some control parameter, one can gradually reduce the affinity of the polymer to the water-oil interface, one moves into the direction of the wetting transition. Exactly when the critical adsorption of the polymer for the water-oil interface is reached, one finds the wetting transition.

There are good reasons to believe that for neutral polymers the wetting transition is second order, and there is no prewetting line associated with the detachment of the water-oil interface from the polymer brush. As soon as the water-oil interface is not reached by the grafted polymer chains, there is no free energy contribution of the substrate any more and the wetting film thickness can diverge smoothly (in the regime of vanishing van der Waals forces, i.e., when the substrate is a solvent-swollen polymer gel). In summary, there might be a prewetting-like line in the wetting phase diagram, but this line is not connected to the wetting transition in this system. This feature is found as well in wetting phase diagrams of the PE brush. At this point it should be mentioned that, formally, the terminology that a prewetting line is not connected to a wetting transition is potentially confusing. We will however use this terminology below to emphasize that the surface phase transitions occur off coexistence (hence, the prefix “pre”).

In the present paper, we will focus on a polyelectrolyte brush because we expect qualitatively different behavior for this system. The reason for this is the following. A polyelec-

trolyte brush in excess solvent (water plus ions, i.e., an electrolyte solution) has at its periphery a diffuse part of the electric double layer, i.e., a Gouy-Chapman layer [11]. To understand the order of the wetting transition, one should focus on the detachment of the electrolyte-oil interface from the polymer brush. Because of the diffuse electric double layer, this should be a favorable process even after the brush chains have stopped forming bridges between the grafting surface and the water-oil interface. With increasing thickness of the water film one will provide the Gouy-Chapman layer with more space (in the water phase) and this will effectively contribute to a repulsive force, pushing the water-oil interface away from the PE brush. Because of this, we expect that the wetting transition for the PE brush is not second order, as for neutral polymer brushes, but first order. If this is true, we anticipate finding a classical prewetting line in the wetting phase diagram that is connected to the wetting transition. In summary, there must be a prewetting line that is linked to the short-range interactions and a prewetting line linked to the detachment of the oil-water interface from the brush. A detailed model is needed to determine which of the two is the leading one that determines whether the system is wet or not.

We use a molecularly realistic self-consistent field (SCF) theory capable of accurately modeling the relevant phenomena anticipated at above. The model can accommodate the phase equilibrium between the two solvents. It is able to capture the formation of a brush and the adsorption of brush chains onto a oil-water interface. It accounts for the electrostatic effects generated by the charged groups in the PE brush. The theory also describes the salt ions in the system that are needed to provide screening of the charges. All these effects are essential elements in the analysis of the wetting phase diagram. More specifically, we will be working with an annealed PE brush for which the charge on the polymer chains depends on the pH of the solution, the local concentration of ions, and also on the dielectric permittivity of the medium. The instrument used to construct the wetting phase diagram is the analysis of adsorption isotherms (at fixed ionic strength, pH , and grafting density, etc.).

In the following we will outline the SCF theory (all approximations are mentioned relatively briefly), and give the values of the parameters of the model when these are first introduced. We will focus on a particular set of parameters that serves our goal. Indeed, we choose, e.g., one special pH value, and all but one of the interaction parameters are fixed to some reasonable value. We haste to mention that these parameters are such that they may well be realized in experiments, but we do not insist on them. It is also understood that qualitatively the same behavior is found for, e.g., different pH values. Of course, one then has to adjust the ionic strength and possibly also tune the interaction parameters with the surface, etc., to return to the same type of the free energy landscape. In this paper, we are interested in the crossing of two prewetting lines in a wetting phase diagram, a phenomenon that is possible when two competing first-order wetting transitions respond differently to a single control parameter. In other words, we will focus on the collection of possible phase portraits.

II. SCF THEORY, THE MOLECULAR MODEL, AND ITS PARAMETERS

In this paper, we use a SCF theory for an annealed polyelectrolyte brush composed of end-grafted chains with pH -dependent charges in a binary liquid that has a solubility gap (water and oil). The control parameter for the wetting phase diagram is the volume fraction of ions in the bulk solution. In the present case, the bulk is the oil phase and it is understood that fixing the ionic strength in the oil phase will induce a much higher ionic strength in the water phase, which will appear as a wetting film inside the brush. The salt partition coefficient, which gives the ratio between the concentration of ions in the water-rich and oil-rich phases, is simply related to the corresponding interaction parameters that specify the solvation of ions in both the water and oil phases.

As analytical solutions are not within reach, we have to resort to numerical solutions of the SCF equations. For this we need a discretization scheme. We use the Scheutjens-Fleer method for this [12–15]. The present problem brings a large number of issues together, but all of them have been discussed before in the open literature. We feel that it is not necessary to go into full detail of the theory here. When we lay down the molecular model we will explain briefly how the SCF model deals with the degrees of freedom in the system and how it accounts for various interactions.

We consider a half-infinite space next to an impenetrable solid boundary. The surface is referred to as S . Although it is an approximation in many systems, we take the surface to be relatively hydrophilic and uncharged. Next to the surface, we have parallel layers of lattice sites with characteristic length $b=0.3$ nm (based on the size of water molecules). The layers are numbered $z=1, \dots, M$, where typically $M=200$. At the system boundary, the bulk conditions are found and boundary effects are minimized by invoking mirrorlike reflecting boundary conditions. Formally, we thus use a pair of surfaces a distance $H=400b$ apart.

The PE brush is assumed to be composed of a string of acid groups [16]. These segments have the generic name A , and the segments occur in two possible states $A_1 \equiv \text{HA}$ and $A_2 \equiv A$ or generally A_k , where $k=1, 2$. These segments are in equilibrium through the reaction $\text{HA} + \text{H}_2\text{O} \rightleftharpoons A^- + \text{H}_3\text{O}^+$ with an equilibrium constant $pK_A=6$ (for concentrations in dimensionless units; 55 moles of water correspond to a volume fraction of $\varphi_W=1$). At this point, it is clear the valence $v_{A1}=0$ and $v_{A2}=-1$. Water W occurs in three states $W_1 \equiv \text{H}_2\text{O}$, $W_2 \equiv \text{OH}^-$, and $W_3 \equiv \text{H}_3\text{O}^+$ with the equilibrium dimensionless constant $pK_W=17.5$, wherein the valences $v_{W1}=0$, $v_{W2}=-1$, and $v_{W3}=1$. All other segments have one state: $k=1$. We consider monovalent salt Na with valence $v_{\text{Na}}=1$ and Cl with valence $v_{\text{Cl}}=-1$, and finally a monomeric apolar monomer with generic name B . As a result the segment types are $X=S, W, \text{Na}, \text{Cl}, A, B$.

Within the layers of lattice sites we are going to implement a mean-field approximation, which allows us to specify the volume fraction of each species $\varphi_X(z)$. Characteristic for a SCF theory is that conjugated to the segment volume fractions there are self-consistent potentials $u_X(z)$. Most of the contributions in the potential $u(z)$ are local, i.e., they depend

on the properties at the coordinate z . However, in wetting problems it is essential that nonlocal contributions, terms that depend on $z' \neq z$, are included as well. These nonlocal contributions arise, e.g., from the fact that segments interact with neighbors that sit on different coordinates. These nonlocal effects are included using the so-called site fractions and are depicted by angular brackets. For some quantity $P(z)$, we write

$$\begin{aligned} \langle P(z) \rangle &= \lambda_1 P(z-1) + \lambda_0 P(z) + \lambda_1 P(z+1) \\ &\approx P(z) + \lambda_1 \frac{\partial^2 P(z)}{\partial z^2}. \end{aligned} \quad (1)$$

The λ parameters present the *a priori* probability to find a neighboring lattice site in the same layer λ_0 or in an adjoining layer λ_1 .

We present the full expression for the segment potentials [16–18] and use the opportunity to mention the interactions that are accounted for in the SCF theory. The segment potential u_{Xk} , which is the free energy needed to bring a segment from the bulk (where the potential is zero) to the coordinate, and the corresponding Boltzmann weight $G_{Xk}(z)$ depends both on the segment type X as well as on the internal state k of the segments

$$\begin{aligned} -\ln G_{Xk}(z) &= u_{Xk}(z) = u'(z) + \sum_{Y,l} \chi_{XkYl} \langle \varphi_{Yl}(z) - \varphi_{Yl}^b \rangle \\ &\quad + v_{Xk} \Psi(z) - \frac{1}{2} \epsilon_0 (\epsilon_X - 1) E^2(z). \end{aligned} \quad (2)$$

The first term in (2) is a Lagrange field coupled to the incompressibility constraint $\sum_X \varphi_X(z)=1$. Physically this contribution is the work needed to create space at coordinate z such that a segment can be inserted. As all segments are of the same size, the value of $u'(z)$ does not depend on the segment type nor the internal state in which the segment is.

The second term in (2) accounts for the short-range interactions between molecular species, which is implemented using the Bragg-Williams approximation. The angular brackets (essential for the modeling of the water-oil interface) are needed to account for the nonlocal nature of the interactions. The Flory-Huggins parameters give the strength of interactions [19]. In an incompressible system, it suffices to specify these parameters only for unlike contacts and these may also depend on the internal state. In principle, there are eight types of distinct segment states in the solution which gives 28 independent FH parameters. As can be seen in Table I, we use only a small number of different parameters. In most cases, we do not make a distinction in what state a segment is. Only for the acid groups we take it that the charged component is strongly repelled by the oil phase and the oil is an athermal (good) solvent for the uncharged segment. Referring to Table I, we have chosen for the following parameters. All charged segments and the water molecules are repelled equally strong from the oil phase. This leads to a binodal value $\varphi_W^\# \approx 0.03787$. The polymer units have θ conditions $\chi=0.5$ with the water molecules and the small ions. For various water soluble PE systems, this setting is a reasonable choice. We assumed that the ions are ideally solvated by

TABLE I. Compilation of the short-range FH interaction parameters, the valences, and the relative dielectric constants. In the final column, the alternative names for the various components is presented for ease of reference.

χ	S	H ₂ O	OH ⁻	H ₃ O ⁺	Na	Cl	AH	A	B	ν	ϵ	Alias
S	0	-1	-1	-1	0	0	0	0	0	0	80	Surface
H ₂ O	-1	0	0	0	0	0	0.5	0.5	3.5	0	80	W ₁
OH ⁻	-1	0	0	0	0	0	0.5	0.5	3.5	0	80	W ₂
H ₃ O ⁺	-1	0	0	0	0	0	0.5	0.5	3.5	0	80	W ₃
Na	0	0	0	0	0	0	0.5	0.5	3.5	1	5	Kation
Cl	0	0	0	0	0	0	0.5	0.5	3.5	-1	5	Anion
AH	0	0.5	0.5	0.5	0.5	0.5	0	0	0	0	2	A ₁
A	0	0.5	0.5	0.5	0.5	0.5	0	0	3.5	-1	2	A ₂
B	0	3.5	3.5	3.5	3.5	3.5	0	3.5	0	0	2	Oil

water. In experimental situations, the ions may not necessarily be ideal. We refrain from these complications here. As the surface has a fixed density [$\varphi_S(0)=1$], we need, in principle, to specify eight interactions with the surface and it is possible to set, e.g., $\chi_{SB}=0$ as the reference for the surface contact. As can be seen in Table I, for simplicity, we only introduced a nonzero adsorption energy for the water component. The default value is $\chi_{WS}=-1$, but we will show the effect of small variations for this interaction strength.

The third term in the segment potential (2) is the classical electrostatic one. Here we use the dimensionless electrostatic potential $\Psi \equiv e\psi/(k_B T)$, where e is the elementary charge and ψ the electrostatic potential in volts. The value of the valence ν_{Xk} depends on the segment and on the internal state (see Table I) and was introduced above already. The electrostatic potential is found from the Poisson equation

$$\frac{\partial}{\partial z} \epsilon(z) \frac{\partial \psi}{\partial z} = - \frac{q(z)}{\epsilon_0} \quad (3)$$

when the charge density distribution $q(z) = \sum_{X,k} e \nu_{Xk} \varphi_{Xk}(z)$ and the relative dielectric permittivity profile $\epsilon(z) = \sum_X \epsilon_X \varphi_X(z)$ are known. In the latter equation, we used the ansatz that a volume fraction weighted average is a reasonable approximation for this profile. The segment-type-dependent quantities are listed in Table I. In short, we have implemented a default value of $\epsilon=80$. The oil, the polymer, and the ions are taken to deviate from this, where for the first two, a value of 2 and for the ions a value of 5 is chosen (quite arbitrarily). The latter value is expected to be of minor importance because basically in the oil phase the dielectric constant is dominated by the B units and the dielectric constant is low. In the aqueous wetting film, the relative dielectric constant will be close to 80 because water will dominate here. The volume fraction weighted average will provide a reasonable intermediate value at the oil-water interface. We note that a discrete version of Eq. (3) is implemented on the lattice, which correctly accounts for the variations of the dielectric permittivity.

The fourth term in Eq. (2) is needed because there are gradients in the dielectric permittivity in the system. It accounts for the fact that molecules are polarized in regions

with an electric field $E \equiv -\partial\psi/\partial z$. In short, the dipole induced by the field is proportional to the electric field, and the energy gain (hence, the minus sign) is also proportional to the electric field, hence, the E^2 dependence. The factor of 1/2 corrects for the fact that there is an entropy loss due to the polarization.

The remaining property of the system that needs to be discussed is the evaluation of the volume fractions for given segment potentials. For this, it is convenient to define segment weighting factors $G_X(z) = \sum_k \alpha_k^b G_{Xk}(z)$, where α_k^b is the probability that a segment is in state k when it is placed in the bulk solution, i.e., in the absence of the electrostatic potential, electric fields, etc. This quantity is, in our case, only a function of the pH and pK values. Of course $\sum_k \alpha_k^b = 1$ in all cases. For the monomeric components the volume fractions are found from $\varphi_X(z) = \varphi_X^b G_X(z)$, and the state dependent distributions follow from $\varphi_{Xk}(z) = \alpha_{Xk}(z) \varphi_X(z)$. It is relatively simply seen that $\alpha_{Xk}(z) = \alpha_{Xk}^b G_{Xk}(z) / G_X(z)$.

For the chain molecules, it is necessary to account for the grafting requirement of the first segment of the chain and for the conformational degrees of freedom. Such computations require enormous CPU time if all chains must be self-avoiding. However, when the chains become strongly stretched, the self-intersecting is not very likely and one can safely go to a more primitive chain model. More specifically we have implemented the freely jointed chain model because for this an efficient method is available to evaluate the single chain partition function. Let the chain have segments with segment ranking numbers $s=1, \dots, N$ (all segments are of the type A), below we will use $N=100$, then the volume fraction distribution of segment s is found by

$$\varphi(z,s) = \frac{\sigma}{G(N|1,1)} \frac{G(z,s|1,1)G(z,s|N)}{G_A(z)}, \quad (4)$$

where σ is the number of chains per unit area. We will fix this quantity to $\sigma=2/100$ such that the chains are well in the brush regime. Equation (4) features the Green's function of the type $G(z_s, s|z_t, t)$, which is interpreted as the statistical weight of all possible and allowed conformations that start with segment $s'=t$, which is at coordinate z_t and ends with segment $s'=s$ at coordinate z_s . If in such a Green's function

a coordinate is missing, it is understood that the integration over this coordinate has been performed, i.e., $G(N|1,1) = \sum_z G(z,N|1,1)$. Indeed, $G(N|1,1)$ contains the statistical weight of all possible conformations that start with segment $s=1$ just next to the surface $z=1$, and this is the single chain partition function. The subpartition functions that occur in Eq. (4) are generated by a propagator scheme

$$G(z,s|1,1) = G_A(z) \langle G(z,s-1|1,1) \rangle \quad (5)$$

$$G(z,s|N) = G_A(z) \langle G(z,s+1|N) \rangle, \quad (6)$$

and these are started using $G(z,s|1,1) = G_A(z) \delta(z,1)$, where $\delta(z,1) = 1$ when $z=1$ and zero; otherwise, $G(z,N|N) = G_A(z)$ for all z , respectively. These propagators are the discrete counterparts of the continuous Edwards diffusion equation [20].

We have discussed how the segment potentials follow from the segment volume fractions and how the volume fractions are computed from the segment potentials. The mutual consistency is enforced by some numerical algorithm. This algorithm operates under a few constraints, namely, that the bulk solution is completely filled by (in this case monomeric compounds, i.e., $\sum_{X \neq S,A} \varphi_X^b = 1$, and that the bulk is electro-neutral, i.e., $\sum_Y \varphi_Y v_Y = 0$, where $Y = \text{Na}, \text{Cl}, W_2, W_3$). The electroneutrality of the system itself remains zero by enforcing the Poisson equation with the reflecting boundary condition at $z=M$, where $E(M)=0$. We choose $\lambda_1 = \lambda_0 = 1/3$. All numerical results have at least seven significant digits.

III. RESULTS AND DISCUSSION

In this section, we will present a set of selected results aimed to illustrate the complexity of the wetting phase diagram in the case of the polyacid brush in a mixed solvent. In particular, our interest is in the parameters near the wetting transition, especially those parameter for which the surface is just wet. Adsorption isotherms should therefore diverge as the chemical potential of the wetting component, which is the water component, approaches the bulk binodal.

Let us first discuss a typical adsorption isotherm for $\varphi_s^b \equiv \varphi_{Cl}^{(oil)} = \varphi_{Cl}^b = 4 \times 10^{-7}$ and $\alpha_{W3}^b = 10^{-9}$ (recall $W_3 = \text{H}_3\text{O}^+$). The first quantity determines the ionic strength, and the second one fixes the chemical potential of the protons and thus the pH to a value near the neutral pH value. In Fig. 1(a), we present the adsorbed amount of water as a function of the logarithm of the bulk volume fraction of water (in the oil phase), and in Fig. 1(b), the corresponding free energy per unit surface area again as a function of the volume fraction of solvent in the (oil) phase.

Referring to Fig. 1(a), it is seen that the adsorption isotherm features a pair of van der Waals loops. The loop at low adsorbed amounts has one spinodal point at supersaturated concentrations well above the φ_W^b values presented in this figure. The second spinodal at subsaturated volume fractions is at $\varphi_W^b \approx 0.03739$. The binodal, which connects a system with just a gas of water molecules at the surface with a microscopic water film, occurs at $\varphi_W^b \approx 0.03765$. Then a second van der Waals loop is found that represents a surface

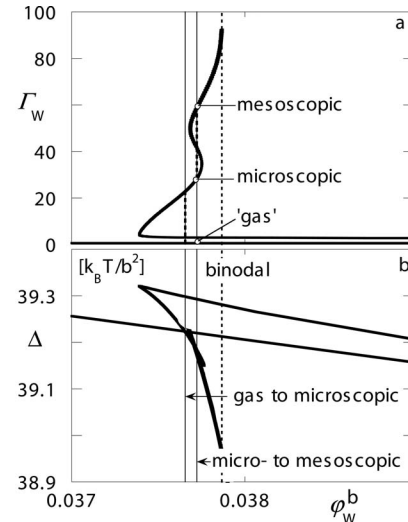


FIG. 1. (a) The adsorbed amount of water Γ_W as a function of the logarithm of the bulk volume fraction of water (in the oil phase) φ_W^b . Three points are indicated on the adsorption isotherm at one value of φ_W^b typical for the “gas” phase, the microscopically thin film, and the mesoscopically thin film. (b) The surface free energy Δ in units of $k_B T / b^2$ as a function of φ_W^b . The dotted vertical line correspond to the bulk binodal $\varphi_W^{\#} = 0.03787$. The vertical line with label “gas to microscopic” is place at $\varphi_W^b = \varphi_W^{*} = 0.03765$, where the first step in the adsorption isotherm occurs. The vertical line with label “micro-” to “mesoscopic” is place at $\varphi_W^b = \varphi_W^{**} = 0.0377$, where the second step in the isotherm occurs.

phase transition that is only weakly first order. Two spinodal points bracket a binodal found at $\varphi_W^b \approx 0.0377$ and connects a microscopically thin water film with a mesoscopically thin one. The adsorption isotherm smoothly diverges upon the approach of the volume fraction of water in the bulk toward the binodal value. This indicates that for the present set of parameters the surface is wet. The two van der Waals loops are connected to the two types of interaction with the substrate. The one at the lower adsorbed amount is linked to the affinity of water for the substrate. In the absence of the brush, this loop must have caused the first-order wetting transition in the system. The second loop is associated with the detachment of the water film from the brush. Again, the fact that there is a loop in the isotherm is the direct proof that the wetting transition is first order when the detachment of the brush chains from the oil-water interface is the most significant event. The steps at φ_W^{*} and φ_W^{**} in combination with the value of the control parameters (φ_s^b or χ_{SW}) are points on prewetting lines in the wetting phase diagrams presented in Figs. 4–7.

In the adsorption isotherm, we have marked three points for the bulk volume fraction of φ_W^b , the first one is characteristic for the molecularly distributed water molecules (gas) at the surface, the second one is labeled “microscopic,” and the third one is called the mesoscopic film. More detailed information for these points are given in Figs. 2 and 3. Before discussing these, we like to point to Fig. 1(b), in which the characteristic surface free energy Δ is presented as a function of the logarithm of the bulk volume fraction of water. Here, $\Delta = F - \sum_i n_i (\mu_i - \mu_i^{\#})$ where F is the Helmholtz en-

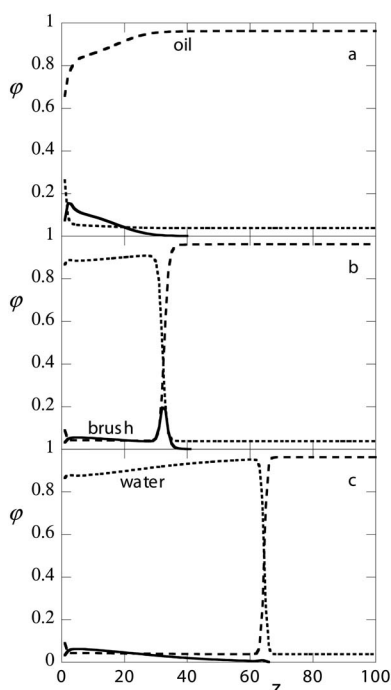


FIG. 2. The volume fraction profile of the brush (solid line), the water (short dashed line), and the oil (long dashed line) for (a) the gas phase, (b) the microscopically thin film, and (c) the mesoscopically thin film at the points indicated in the adsorption isotherm of Fig. 1(a) for the stable surface layers at $\phi_W^b = 0.0377$. All parameters as in Fig. 1.

ergy and the sum runs over all molecular components i that are not grafted. For full details, we refer to the literature [15]. For each van der Waals loop [of Fig. 1(a)], there is a cusped figure in Fig. 1(b). The spinodal points represent the cusps. The crossing of the lines points to the binodal. The binodal is either located by the plot of the surface free energy versus the (logarithm) phibulk of the solvent or by some equal area construction using the van der Waals loops of Fig. 1(a). The first procedure is the simplest and the most accurate.

Space does not allow us to analyze in full depth the structure of the polymer brush in the mixed solvent systems. We have visited this problem extensively in other publications and refer to these works for more details [21]. Nevertheless, it is instructive to briefly give some insight into the structure of the interface at some characteristic points along the adsorption isotherm. The stable parts of the adsorption isotherm are characterized by $\partial \Gamma_w / \partial \ln \phi_w^b > 0$. Indeed, there are three regions of stability. In the first stable region of the isotherm, there is just a minute amount of water at the substrate. Hence, we call this the gas-phase solution. The profile of water, oil and polymer is given in Fig. 2(a). (This result is typical for all surface states labeled “gas,” which are discussed below.) The corresponding electrostatic potential profile is presented in Fig. 3(a), and the distributions of the two types of ions are presented in Fig. 3(b). The polymer is mostly in the oil phase, while the profile has clearly a parabolic shape. Only in the thin water layer near the surface has some polymer segment accumulated, and one finds polymer segments that are dissociated. Because of the low dielectric

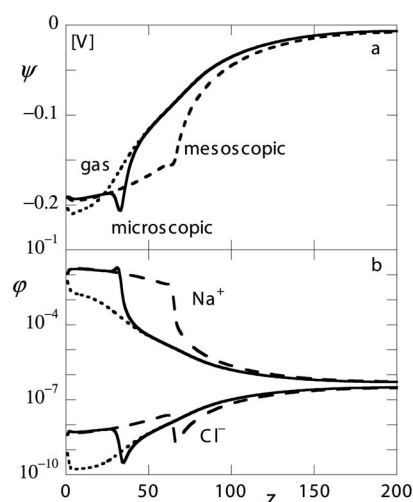


FIG. 3. (a) The electrostatic potential profile corresponding to the three indicated points on the adsorption isotherm of Fig. 1, the gas (short dashed line), the microscopic (solid line), the mesoscopic thin (long dashed line) film for the stable surface layers at $\phi_W^b = 0.0377$. (b) The corresponding distributions of the 1:1 electrolyte ions in log-lin coordinates.

constant, these few charges generate a very large electrostatic potential of approximately $\psi = -200$ mV, which decays very slowly in the oil phase.

The second part of the isotherm with a stable amount of water in the brush is found when the water film is 3–35 lattice layers thick (1–10 nm). We will refer to this solution as the microscopically thin water film. A typical example for all surface states to be referred to as “mesoscopic” is shown in Fig. 2(b). Here various chains “travel” from the surface to the oil-water interface. The bridging chains are more or less homogeneously stretched (the profile is nearly flat). At the oil-water interface a significant adsorption of polymer units is found. Such conformations are typically referred to as flowerlike in the literature [7]. The electrostatic potential in the water film is more or less homogeneous [cf. Fig. 3(a)], and the water film is loaded with counterions [cf. Fig. 3(a)]. The locally high counterion concentration is caused by the high electrostatic potential in the water phase. Even though there are many more charged polymer segments, the maximum electrostatic potential did not change much with increasing water content.

The third part of the isotherm with a stable amount of water near the surface is found for film thicknesses in excess of 15 nm. We will refer to these states as the mesoscopically thin film. The result of Fig. 2(c) is a typical example for which a few polymer chains still touch the oil-water interface. The electrostatic potential is high throughout the strongly stretched brush chains, and the counterion concentration is high as in the previous case. Both brush profiles in Figs. 2(a) and 2(c) are mostly in a homogeneous medium. The two profiles differ enormously. Indeed, when the brush is in the oil, the chain is uncharged and the neutral parabolic shape is found. When the brush is in the water phase, it is mostly charged and the counterions that compensate most of the brush charges cause a local high osmotic pressure such that the polymer brush is highly swollen.

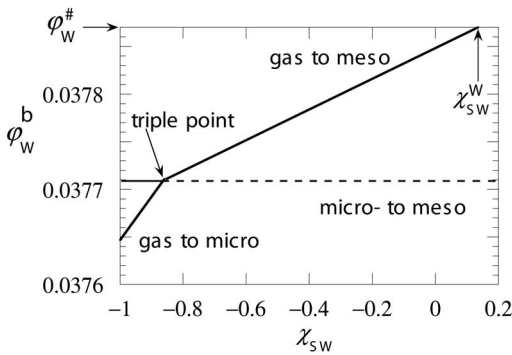


FIG. 4. Wetting phase diagram in the coordinates ϕ_W^b where the steps occur in the isotherm as a function of the affinity of water for the surface χ_{SW} . All other parameters are the same as in Fig. 1. The crossing of the (prewetting) lines occurs at a triple point (where three surface layers coexist) is indicated. The line labeled gas-meso(scopi) hits the bulk binodal ($\phi_W^{\#}$ indicated with a horizontal arrow) at $\chi_{SW}^W = \chi_{SW}^{\text{triple}} \approx 0.135$ (indicated by a vertical arrow). The microscopic-to-mesoscopic transition is only a stable transition when $\chi_{SW} < \chi_{SW}^{\text{triple}}$. For the lower adsorption affinities, this loop occurs in a metastable branch of the other transition and we dotted this transition line. The transition from gas to microscopic changes at the triple point into the gas to mesoscopic one. Note the change in slope of this prewetting line at the triple point.

For the line of arguments, it is significant to mention that in all three cases presented above there exists a significant diffuse electric layer on top of the water film inside the oil phase. Indeed, it would be much better for the system to have the diffuse double layer fully inside a medium with a high dielectric permittivity. Consistent with this, we find that the adsorbed amount of water Γ_W becomes a steeply increasing function of the bulk concentration of water (cf. Fig. 1); indeed, it diverges upon the approach of $\phi_W^{\#}$.

It is significant to know how the adsorption isotherms change as a function of some of the parameters in the system. We first consider the affinity of water for the surface. This affinity is given by the χ_{SW} parameter. This short-range interaction parameter can only influence the adsorption isotherms for low adsorbed amounts, i.e., it can only influence the position of the lower van der Waals loop, that is for low values of Γ_W . This is in line with the wetting phase diagram presented in Fig. 4, where the bulk volume fractions ϕ_W^b for which the two loops occur are given as a function of χ_{SW} (the points at $\chi_{SW} = -1$ are extracted from Fig. 1). With decreasing affinity for the surface, the transition point for the lower van der Waals loop shifts to higher ϕ_W^b values. The transition points for the second van der Waals loop are completely unaffected by changes in χ_{SW} . The two lines in this wetting phase diagram cross each other at a triple point. At this point, three surface states coexist, i.e., three surface states are stable solutions for the given bulk volume fraction. The volume fraction profiles shown in Figs. 2 and 3 are very similar to these three surface states: there is the gas, the microscopic, and the mesoscopic film. For $\chi_{SW} > \chi_{SW}^{\text{triple}}$, there is just one observable surface phase transition left in the system, namely, one from the gas to the mesoscopically thin film. The other transition is “hidden” in the loop at subsaturated concentrations of this remaining van der Waals loop. As an

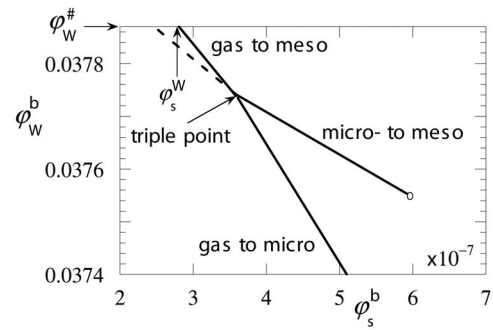


FIG. 5. The wetting phase diagram in the coordinates of the volume fraction of water in the bulk (oil) phase where steps in the isotherm take place as a function of the salt volume fraction in the oil phase. The interaction parameter of water with the surface is fixed to $\chi_{SW} = -1$. The triple point and the wetting transition are indicated. At the triple point, the transition from microscopic to mesoscopic switches from a stable transition to a metastable one (dashed line), and the gas-to-microscopic transition switches to the gas-to-mesoscopic transition. The latter curve is connected to the wetting transition.

equal area construction is still possible for this metastable loop, we have dotted this microscopic-to-mesoscopic transition in Fig. 4. With decreasing affinity, the loop labeled gas to mesoscopic hits the bulk binodal at the wetting transition value $\chi_{SW}^W \approx 0.135$. At extremely negative values of χ_{SW} , far outside the plotted range, there is a critical endpoint of the gas-to-microscopic phase transition.

Potentially more exciting wetting phase diagrams are expected when it is possible to influence both (prewetting) transitions with the same control parameter. Both the microscopically thin as well as the mesoscopically thin film are characterized by a locally dissociated polymer brush, which necessarily will respond to the ionic strength. Also the formation of the gas phase is likely to respond to the ionic strength. As a result, the ionic strength, given by ϕ_s^b , is a natural control parameter to influence both transitions. In Fig. 5, the wetting phase diagram is shown wherein the ionic strength in the oil phase was used as the control parameter. Again, we mention that the total volume fraction of counterions in the water film (inside the charged brush) is many orders of magnitude larger. As can be seen from Fig. 5, for which the interaction of water for the surface was fixed to $\chi_{SW} = -1$, we find once again two crossing lines. A line in a wetting phase diagram represents a surface phase transition. The labeling of the lines is identical to that in Fig. 4. Indeed, both transitions show a clear response on the change of the ionic strength. With increasing ionic strength, the system approaches the wetting condition. In this case, the wetting transition is found to be $\phi_s^W \approx 3.8 \times 10^{-7}$. Again, the two prewetting lines cross at a triple point where the gas, the microscopically thin, and the mesoscopically thin films coexist. As in Fig. 4, only one of the prewetting lines is linked to the wetting transition. It is the line that is labeled “gas to microscopic” above the triple point and “gas to mesoscopic” below the triple point. The prewetting line with the label “microscopic to mesoscopic” is observable above the triple point, but becomes within the van der Waals loop of the

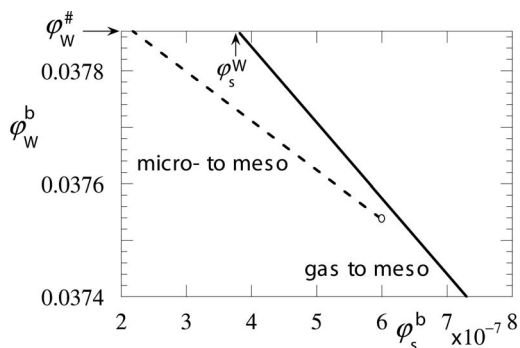


FIG. 6. The wetting phase diagram as $\phi_W^b(\phi_s^b)$, similar to the one presented in Fig. 5 with the same parameter setting except $\chi_{SW}=0$.

other transition below the triple point. Hence, we have dashed this curve in this region. The critical end point of the microscopic-to-mesoscopic transition occurs near the triple point, i.e., at $\phi_s^b \approx 6 \times 10^{-7}$. The critical point of the other prewetting line is far outside the plotted region at $\phi_s^b \approx 6 \times 10^{-6}$. The prewetting lines are nearly straight lines; however, at the triple point they change their slopes.

For the next wetting phase diagram, presented in Fig. 6, we have changed the affinity of the water for the surface and have selected $\chi_{SW}=0$. From the above (cf. Fig. 4), we know that the adsorption energy has the effect near the surface and that the gas-to-microscopic or the gas-to-mesoscopic transition is affected by this and much less the transition from the microscopic to mesoscopic water layers. In general, we thus expect that the triple point moves to higher ϕ_s^b values the lower the short-range affinity of water for the surface. In line with this, one can see in Fig. 6 that the two prewetting lines have shifted with respect to each other to such an extent that they no longer cross each other. In this particular case, the prewetting line representing the microscopic-to-mesoscopic transition is buried completely within the van der Waals loop of the other transition. As before, these transitions are not observable and we therefore have dashed the line. The prewetting line associated to the wetting transition at $\phi_s^b \approx 3.78 \times 10^{-7}$ represents the jump in the adsorbed amount of the water component from the gas phase directly into the mesoscopically thin film. Both prewetting lines are, to a good approximation, straight lines, and the critical end point of the “hidden” transition is again near $\phi_s^b \approx 6 \times 10^{-7}$. It is perfectly possible to find some value for the adsorption energy χ_{SW}^* , for which the prewetting line for the gas to mesoscopic layer transition is touching the hidden prewetting line such that the critical endpoint occurs at the same ionic strength as the first-order transition due to the surface interactions. From the results, we may estimate this adsorption energy to be slightly below zero, i.e., $\chi_{SW}^* \approx -0.1$.

With increasing affinity of the water for the surface, i.e., more negative χ_{SW} values, we expect the shift of the triple points toward lower ionic strength. To illustrate that this is possible, we present the final wetting phase diagram for the case that $\chi_{SW}=-1.5$ in Fig. 7. We have chosen χ_{SW} such that the two prewetting come together near the wetting transition. Unlike in Fig. 6, both prewetting lines are experimentally observable. This means that we can have adsorption iso-

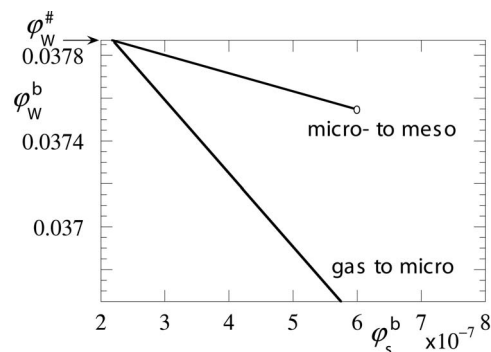


FIG. 7. The wetting phase diagram as $\phi_W^b(\phi_s^b)$, similar to the one presented in Fig. 5 with the same parameter setting except $\chi_{SW}=-1.5$.

therms with two consecutive steps. The first one is from the gas to the microscopically thin water layer, the second from the microscopic thin to the mesoscopic thin layer. As the wetting transition is associated with the transition at the longer length scale, it is the latter that is connected to the wetting transition. In this particular case, the wetting transition is found for $\phi_s^b \approx 2.2 \times 10^{-7}$.

As shown in Fig. 6, it is possible to find a value for the adsorption energy of water for the surface χ_{SW}^* such that the two prewetting lines intersect exactly at the wetting transition point. In this case, the triple point and the wetting transition coincide. In this system, this occurs for χ_{SW} extremely close to $\chi_{SW}^*=-1.5$.

For the case that $\chi_{SW} < -1.5$, we find detached prewetting lines. Interestingly, in this regime of adsorption energies the wetting transition becomes independent of the strength of which the solvent is attracted to the surface. For values of the ionic strength less than the wetting transition, i.e., for $\phi_s^b < 2.2 \times 10^{-7}$, the system is in the partial wetting regime. Interestingly, one may still find the prewetting step from the gas to the microscopically thin film in an adsorption isotherm for such low ionic strength cases. However, in such a case the water film will not grow to macroscopic sizes when the bulk binodal is reached at $\phi_W^{\#}$. This phenomenon was also found for the neutral polymer brush for a large range of values of the control parameter [8] and is related to results for the wetting of alkanes of the air-water interface in the presence of surfactants. Here this phenomenon is referred to as pseudopartial wetting [9,10].

In summary, we have shown that a polyacid brush can be wetted by salty water from an apolar (oil) phase. The brush presents interactions to the electrolyte solution on two length scales. The short-range interactions with the surface can compete with the longer-range interactions that have to do with the solvation of the polyacid brush. We have seen that the wetting transition in these systems is first order. It is possible to have wetting transitions that are controlled by the short-range surface interactions and wetting transitions that are linked to the detachment of the water-oil interface from the charged brush. This intricate behavior has various unusual consequences. One of these is that there are two prewetting lines in the wetting phase diagram, whereas there is just one wetting transition.

Above we have shown that it is possible to find a set of parameters for which the two prewetting lines cross each other in the wetting phase diagram at a triple point. It is possible to collect all possible triple points in the system. These triple points all lay on the dashed line of Fig. 6. In general, the triple points have very special implications. At the triple point, three surface states coexist. This means that on the surface one should find, at such special point, locally a very thin film (gas), somewhere else a microscopically thin film and again somewhere else a mesoscopically thin film, all in mutual equilibrium.

For another interesting consequence, we return to Fig. 7. For the ionic strength $\varphi_s^b < 2.2 \times 10^{-7}$, the system is in the partial wetting regime. The prewetting line labeled “gas to microscopic” can still reach $\varphi_w^\#$, e.g., for a particular value of the adsorption energy $\chi_{SW}^\# = \chi_{SW} < -1.5$. As the surface is nonwet, it means that a macroscopic drop of electrolyte solution meets the interface with a finite contact angle. At the three-phase contact line, we can now have two coexisting film thicknesses. One may be identified by the microscopically thin film and the other one is the gas phase. This result is a natural consequence for the pseudopartial wetting phenomenon, and for related systems, there may be experimental evidence that this effect can indeed occur [5].

When an electrolyte solution is presented to a polyacid brush when the surface is wet (i.e., for $\varphi_s^b > 2.2 \times 10^{-7}$), a thick wetting layer should form. Close enough to the wetting transitions, there are however a few surface phase transitions that may present kinetic barriers. First-order surface phase transitions have metastable branches associated with these, and we may expect to have significant hysteresis effects in the formation of the wetting films. The complexity of the wetting phase diagram has been outlined above, and this may help us to understand it. We hope that our theoretical analysis will stimulate experiments in this direction.

IV. CONCLUSIONS

Using a detailed self-consistent field theory, we were able to generate a set of portraits of the wetting phase diagram of a polyacid brush wetted by an electrolyte solution. We argued that the electrolyte solution sees two types of interaction in this system. Both interactions have the intrinsic possibility to generate a first-order wetting transition in this system. For very strong water-surface affinity, we have shown that the wetting transition is just a function of the ionic strength. A high enough ionic strength enables the

polyacid chain to dissociate freely in the aqueous water film. This dissociation promotes the wetting. The electric double layer above the surface gives a repulsive contribution that thickens the wetting film because it favors the water-phase over the oil phase. When the water-surface interaction is only marginally strong, the wetting transition becomes under control of this parameter. Because the water-oil system is far from its critical conditions, therefore the wetting transitions are again first order. The portraits feature two prewetting lines connected to the two types of interaction. The lines can be separated, but they can also cross each other. The crossing point represents a triple point for which there are three film thicknesses coexisting at the surface at some bulk volume fraction of water less than the bulk binodal: (i) There is the gas phase, for which there is very little water at the surface and the polymer brush is in the neutral state with a parabolic profile, i.e., apart from the hump near the surface ($z < 5$) and the exponentially decaying profile for $z > 25$, the profile can be fitted by a parabola [$\varphi(z) \propto H^2 - z^2$ where H is a measure of the size of the brush]. (ii) There is the microscopic state, where the brush chains have an inhomogeneous conformation with a strongly stretched stem going from the surface to the oil-water interface and the remaining segments are associated with this L/L interface. (iii) There is the mesoscopically thin adsorbed water layer where the brush is strongly stretched due to the osmotic pressure of the counterions resides completely in the water film. However, the electric double layer is still partly in the oil phase. A complex wetting phase diagram points to the rather rough free energy landscape the electrolyte solution finds itself in when it wets the polyacid brush. Even though the parameters may be such that the surface should be wet, there may be long-lived metastable states of partially developed wetting films. These and other effects should be of interest to experimentalists.

ACKNOWLEDGMENTS

The authors acknowledge financial support from the Dutch National Science Foundation (NWO) and the Russian Foundation for Basic Research (RFBR) through joint Projects No. 047.016.004 “Computational approaches for multi-scale modelling in self-organizing polymer and lipid systems” and No. 047.017.026 “Polymers in nanomedicine: design, synthesis and study of inter-polymer and polymer-virus complexes in search of novel pharmaceutical strategies.” E.B.Z. acknowledges partial support from the Russian Foundation for Basic Research (RFBR Grant No. 05-03-33126).

[1] D. Bonn and D. Ross, *Rep. Prog. Phys.* **64**, 1085 (2001).
 [2] M. A. Cohen Stuart and F. A. M. Leermakers, *Physica A* (to be published).
 [3] M. A. Cohen Stuart, W. M. de Vos, and F. A. M. Leermakers, *Langmuir* **22**, 1722 (2006).
 [4] M. Schick, *Liquids at Interfaces*, edited by J. Charvalin, J. F. Joanny, and J. Zinn-Justin (Les Houches, Amsterdam, 1988).

[5] J. H. Maas, M. A. Cohen Stuart, F. A. M. Leermakers, and N. A. M. Besseling, *Langmuir* **16**, 3478 (2000).
 [6] A. A. Mercurieva, F. A. M. Leermakers, T. M. Birshtein, G. J. Fleer, and E. B. Zhulina, *Macromolecules* **33**, 1072 (2000).
 [7] A. M. Skvortsov, L. I. Klushin, and F. A. M. Leermakers, *Europhys. Lett.* **58**, 292 (2002).
 [8] F. A. M. Leermakers, A. Mercurieva, J. van Male, E. B.

- Zhulina, N. A. M. Besseling, and T. M. Birshtein, *Langmuir* **16**, 7082 (2000).
- [9] N. Shahidzadeh, D. Bonn, K. Ragil, D. Broseta, and J. Meunier, *Phys. Rev. Lett.* **80**, 3992 (1998).
- [10] K. M. Wilkinson, C. D. Bain, H. Matsubara, and M. Aratono, *ChemPhysChem* **6**, 547 (2005).
- [11] J. Lyklema, *Fundamentals of Interface and Colloid Science* (Academic Press, London, 1995), Vol. II.
- [12] J. M. H. M. Scheutjens and G. J. Fleer, *J. Phys. Chem.* **83**, 1619 (1979).
- [13] J. M. H. M. Scheutjens and G. J. Fleer, *J. Phys. Chem.* **84**, 178 (1980).
- [14] G. J. Fleer, M. A. Cohen Stuart, J. M. H. M. Scheutjens, T. Cosgrove, and B. Vincent, *Polymers at Interfaces* (Chapman and Hall, London, 1993).
- [15] O. A. Evers, J. M. H. M. Scheutjens, and G. J. Fleer, *Macromolecules* **23**, 5221 (1990).
- [16] Y. Lauw, F. A. M. Leermakers, M. A. Cohen Stuart, O. V. Borisov, E. B. Zhulina, *Macromolecules* **39**, 3628 (2006).
- [17] M. M. A. E. Claessens, B. F. van Oort, F. A. M. Leermakers, F. A. Hoekstra, and M. A. Cohen Stuart, *Biophys. J.* **87**, 3882 (2004).
- [18] J. F. L. Duval, F. A. M. Leermakers, and H. P. van Leeuwen, *Langmuir* **20**, 5052 (2004).
- [19] P. J. Flory, *Principles of Polymer Chemistry* (Cornell University Press, Ithaca, NY, 1953).
- [20] S. F. Edwards, *Proc. Phys. Soc. London* **85**, 613 (1965).
- [21] A. A. Mercurieva, T. M. Birshtein, E. B. Zhulina, P. Iakovlev, J. van Male, and F. A. M. Leermakers, *Macromolecules* **35**, 4739 (2002).